A Fast Time-Domain Finite Element–Boundary Integral Method for Electromagnetic Analysis

Dan Jiao, Mingyu Lu, Eric Michielssen, *Senior Member, IEEE*, and Jian-Ming Jin, *Fellow, IEEE*

***Abstract*—A time-domain, finite element–boundary integral (FE–BI) method is presented for analyzing electromagnetic (EM) scattering from two-dimensional (2-D) inhomogeneous objects. The scheme's finite-element component expands transverse fields in terms of a pair of orthogonal vector basis functions and is coupled to its boundary integral component in such a way that the resultant finite element mass matrix is diagonal, and more importantly, the method delivers solutions that are free of spurious modes. The boundary integrals are computed using the multilevel plane-wave time-domain algorithm to enable the simulation of large-scale scattering phenomena. Numerical results demonstrate the capabilities and accuracy of the proposed hybrid scheme.**

***Index Terms*—Boundary integral equations, finite element methods, electromagnetic scattering, electromagnetic transient analysis.**

I. Introduction

THE HYBRID finite element–boundary integral (FE–BI) method constitutes a powerful numerical technique for solving open-region electromagnetic (EM) scattering problems. The method separates a region containing the scatterer (interior domain) from the remainder of the space (exterior domain) by an artificial boundary. The fields in the interior and exterior domains are represented in terms of finite elements (FE) and a boundary integral (BI), respectively. These two representations are then matched to each other across the boundary. In the past, the FE–BI scheme has been widely applied to the analysis of two-dimentional (2-D) and three-dimensional (3-D) frequency-domain EM scattering and radiation problems (see [1] and references therein). To the authors' knowledge, however, no time-domain FE–BI scheme has been reported in the open literature. This paper describes an FE–BI scheme for analyzing transient scattering from 2-D freestanding inhomogeneous objects.

Because of their potential to generate wide-band data and model nonlinear materials, numerical schemes for simulating EM transients have grown increasingly popular in recent years. In addition to finite-difference time-domain (FDTD) [2] and time-domain integral equation based schemes [3], two classes of time-domain FE methods (TDFEM) have been proposed [4]–[20]. Schemes in the first class directly discretize Maxwell's equations [4]–[12]; this process typically results in finite difference-like leap-frog schemes that do not leverage our extensive knowledge of frequency-domain FE solvers. Schemes in the second class tackle the second-order vector wave equation, also known as the curl–curl equation, obtained by eliminating one of the field variables from Maxwell's equations [13]–[19]. The principal disadvantage of these approaches is that they require a matrix equation to be solved in each time step. Several lumping methods have been proposed to render this matrix diagonal, thereby obviating the need for inverting it. Unfortunately, these lumping techniques have been found to introduce errors in the finite element solution and for unstructured meshes, the lumping process is likely to produce zero or negative diagonal elements, which results in the definite instability; therefore, they are not recommended for use [20]. A recently developed scheme [18] avoids lumping altogether by constructing orthogonal basis functions that yield a diagonal FE matrix.

An important issue in the construction of FE-based solvers for analyzing open-region scattering problems is the treatment of the artificial truncation boundary. Popular truncation schemes impose an absorbing boundary condition or wrap the computational domain in a perfectly matched layer [21]–[23]. Another approach expresses fields exterior to the truncation boundary in terms of boundary integrals, which leads to the FE–BI method discussed earlier. This approach is exact, and more importantly, it allows the truncation boundary to take on any shape (usually conformal to the outline of the object being studied) and to be placed arbitrarily close to the object, which in turn reduces the required computational and memory resources. As pointed out previously, while this approach is well developed in the frequency domain, it has yet to be exploited in the time domain.

This paper presents a new FE–BI scheme for analyzing transient EM scattering from freestanding inhomogeneous objects. The scheme offers two unique features. The first feature involves the hybridization of the FE and BI components of the solver. Instead of adopting the standard hybridization scheme used in frequency domain, a novel scheme is proposed that preserves the sparseness of the finite element matrix and simultaneously yields solutions free of spurious modes. The second feature is the use of a fast algorithm, viz., the multilevel plane-wave time-domain (PWTD) method, for evaluating the BIs, which greatly reduces the computing time when an object of a large electrical dimension is considered. In addition, we employ a pair of orthogonal vector basis functions, developed by White [18], to obviate the need for a matrix solution in each time step without loss of accuracy.

The proposed FE–BI scheme is described in Section II. Section III demonstrates the capabilities and accuracy of the scheme

Manuscript received June 5, 2000; revised February 6, 2001. This work was supported in part by AFOSR under the MURI Program, under contract F49620-96-1-0025, and in part by Sandia National Laboratory.

The authors are with the Center for Computational Electromagnetics, Department of Electrical and Computer Engineering, University of Illinois at Urbana-Champaign, Urbana, Il 61801-2991 USA.

Publisher Item Identifier S 0018-926X(01)06363-3.

through a host of numerical examples. Finally, Section IV relates our conclusions.

II. Formulation

This section describes a new FE–BI scheme for analyzing 2-D open-region scattering problems. Section II-A defines the problem and introduces notation. Throughout, all fields are assumed to be TMz polarized; the proposed scheme, however, also applies to TEz scattering problems with minimal modifications. The FE–BI scheme, including White's set of orthogonal basis functions [18] and the new coupling scheme, are presented in Section II-B. Finally, Section II-C describes the PWTD-based evaluation of the BIs. Although this 2-D problem can be solved more easily using the axial component of the electric field as the unknown variable, the formulation and implementation are carried out here using the transverse components of the magnetic field so that the method can readily be extended to 3-D vector problems.

A. Problem Statement and Hybridization Scheme

Consider a freestanding inhomogeneous dielectric cylinder with embedded electric and magnetic walls Γ_e and Γ_m that extends along the z-axis. This cylinder is excited by a magnetic field $\mathbf{H}^{\rm inc}(\boldsymbol{\rho},t)=H_x^{\rm inc}(\boldsymbol{\rho},t)\hat{\mathbf{x}}+H_y^{\rm inc}(\boldsymbol{\rho},t)\hat{\mathbf{y}}$ where $\boldsymbol{\rho}=x\hat{\mathbf{x}}+y\hat{\mathbf{y}}$; $\mathbf{H}^{\rm inc}(\boldsymbol{\rho},t)$ is assumed zero throughout the cylinder for $t<0$. The total magnetic field $\mathbf{H}(\boldsymbol{\rho},t)=H_x(\boldsymbol{\rho},t)\hat{\mathbf{x}}+H_y(\boldsymbol{\rho},t)\hat{\mathbf{y}}$ comprises the sum of $\mathbf{H}^{\rm inc}(\boldsymbol{\rho},t)$ and the scattered field $\mathbf{H}^{\rm scat}(\boldsymbol{\rho},t)=H_x^{\rm scat}(\boldsymbol{\rho},t)\hat{\mathbf{x}}+H_y^{\rm scat}(\boldsymbol{\rho},t)\hat{\mathbf{y}}$. In what follows, the cylinder is assumed to be recursively embedded in two domains Ω_s and Ω_o with boundaries Γ_s and Γ_o, respectively (Fig. 1). In addition, position dependent unit vectors normal to Γ_q $(q=e,m,s,o)$ are denoted by $\hat{\mathbf{n}}_q$ (which is assumed outward pointing if Γ_q is closed). Finally, the permittivity, permeability, and conductivity of the cylinder and its surroundings are denoted by ϵ, μ, and σ; they revert to their free-space values ϵ_0, μ_0, and zero outside Γ_s. The spatial dependence of all time-independent quantities is understood and omitted.

In Ω_o, $\mathbf{H}(\boldsymbol{\rho},t)$ obeys

$$\nabla\times\left[\epsilon^{-1}\nabla\times\mathbf{H}(\boldsymbol{\rho},t)\right]+\mu\partial_t^2\mathbf{H}(\boldsymbol{\rho},t)+\mu\sigma\epsilon^{-1}\partial_t\mathbf{H}(\boldsymbol{\rho},t)=\mathbf{0} \tag{1}$$

subject to the boundary conditions

$$\hat{\mathbf{n}}_m\times\mathbf{H}(\boldsymbol{\rho},t)=\mathbf{0},\quad \boldsymbol{\rho}\in\Gamma_m \tag{2}$$

$$\hat{\mathbf{n}}_e\times\left[\nabla\times\mathbf{H}(\boldsymbol{\rho},t)\right]=\mathbf{0},\quad \boldsymbol{\rho}\in\Gamma_e \tag{3}$$

and

$$\epsilon_r^{-1}\hat{\mathbf{n}}_o\times[\nabla\times\mathbf{H}(\boldsymbol{\rho},t)]+c^{-1}\partial_t\{\hat{\mathbf{n}}_o\times[\hat{\mathbf{n}}_o\times\mathbf{H}(\boldsymbol{\rho},t)]\}=\mathbf{V}(\boldsymbol{\rho},t),\quad \boldsymbol{\rho}\in\Gamma_o. \tag{4}$$

The left-hand side of (4) is nothing but a linear combination of the time derivatives of the electric and the magnetic fields tangential to Γ_o. The right-hand side expresses the same quantity in terms of equivalent electric and magnetic sources $\mathbf{J}(\boldsymbol{\rho},t)$ and $\mathbf{K}(\boldsymbol{\rho},t)$ that reside on Γ_s and that are defined as

$$\mathbf{J}(\boldsymbol{\rho},t)=\hat{\mathbf{n}}_s\times\mathbf{H}(\boldsymbol{\rho},t),\quad \boldsymbol{\rho}\in\Gamma_s \tag{5}$$

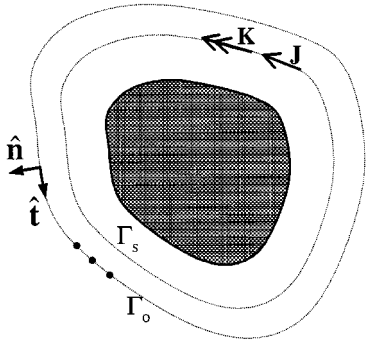

Fig. 1. Illustration of the truncation and source boundaries.

and

$$\mathbf{K}(\boldsymbol{\rho},t)=-\hat{\mathbf{n}}_s\times\left\{\epsilon^{-1}\partial_t^{-1}[\nabla\times\mathbf{H}(\boldsymbol{\rho},t)]\right\},\quad \boldsymbol{\rho}\in\Gamma_s, \tag{6}$$

where ∂_t^{-1} denotes temporal integration. In other words, $\mathbf{V}(\boldsymbol{\rho},t)$ is given by (4) with $\mathbf{H}(\boldsymbol{\rho},t)$ replaced by

$$\tilde{\mathbf{H}}(\boldsymbol{\rho},t)=\mathbf{H}^{\rm inc}(\boldsymbol{\rho},t)+\int_0^t\left(\partial_t^2\bar{\bar{\mathbf{I}}}-c^2\nabla\nabla\right)\cdot\mathbf{F}(\boldsymbol{\rho},t)dt+\nabla\times\mathbf{A}(\boldsymbol{\rho},t) \tag{7}$$

where

$$\mathbf{A}(\boldsymbol{\rho},t)=\mu_0\int_{\Gamma_s}\mathbf{J}(\boldsymbol{\rho}',t)\star g(|\boldsymbol{\rho}-\boldsymbol{\rho}'|,t)d\ell' \tag{8}$$

$$\mathbf{F}(\boldsymbol{\rho},t)=\epsilon_0\int_{\Gamma_s}\mathbf{K}(\boldsymbol{\rho}',t)\star g(|\boldsymbol{\rho}-\boldsymbol{\rho}'|,t)d\ell'. \tag{9}$$

In these equations, $g(|\boldsymbol{\rho}-\boldsymbol{\rho}'|,t)$ denotes the 2-D Green's function

$$g(\rho,t)=\frac{1}{2\pi}\frac{u(t-\frac{\rho}{c})}{\sqrt{t^2-\left(\frac{\rho}{c}\right)^2}} \tag{10}$$

where $u(\cdot)$ is a unit step function.

Before proceeding, it should be noted that the hybridization scheme described above is different from the traditional ones. In the present scheme, the FE and BI components are coupled through (4), whereas, traditional schemes couple the FE and BI components using either the first or the second term of the left-hand side of (4). If only the first term is present, (4) specifies the curl of the magnetic field and, hence, imposes a Neumann condition; in contrast, if only the second term is present, (4) imposes a Dirichlet condition. Although both traditional schemes yield a valid hybridization, they all suffer from the problem of interior resonance associated with the electric and magnetic field integral equations. This problem is well known in the frequency-domain boundary integral equation solvers [24] and it was also observed in our implementations using the traditional hybridization schemes. Indeed, although theoretically the solution to the above boundary-value problem does not support any resonant modes if the system is assumed relaxed at $t=0$, these modes do build up the solution obtained using BI-based schemes if no precautions are taken. To be more specific, when the first (or second) term of (4) is specified, spurious modes that

correspond to the resonant modes of an empty cavity formed by electric (or magnetic) walls of the same shape as Γ_o appear in the numerical solution. These spurious modes corrupt the true solution and cause instabilities in the time marching process.

The proposed hybridization scheme removes the problem of spurious modes by postulating the boundary condition on Γ_o in the form of (4), which involves both the magnetic field and its curl. Careful examination of (4) reveals that this is actually a boundary condition describing an impedance surface whose impedance is that of free space. As a result, the cavity formed by such a surface cannot support real resonance. To a certain extent, the proposed BI formulation resembles that of the combined-field integral equation. In addition to the removal of spurious modes, the use of (4) renders a lossy FE system even if the region Ω_o is lossless. Such a lossy FE system enhances the stability of the time marching process.

It is also worthwhile to note that if the second and third terms (BI terms) on the right-hand side of (7) are neglected, (4) reduces to the standard first-order absorbing boundary condition (ABC). Such an ABC is reflectionless only for the normally incident waves. Clearly, the BI terms provide corrections to the first-order ABC so that (4) becomes an exact ABC.

B. Time-Domain Finite-Element Solution

In accordance with the variational principle [25], solving the boundary-value problem defined by (1)–(4) is equivalent to seeking the zero of the first variation of the functional

$$\begin{aligned} F[\mathbf{H}(\boldsymbol{\rho},t)] =& \frac{1}{2}\iint_{\Omega_o}\Big\{\epsilon^{-1}[\nabla\times\mathbf{H}(\boldsymbol{\rho},t)]\cdot[\nabla\times\mathbf{H}(\boldsymbol{\rho},t)] \\ &+\mu\partial_t^2\mathbf{H}(\boldsymbol{\rho},t)\cdot\mathbf{H}(\boldsymbol{\rho},t) \\ &+\mu\sigma\epsilon^{-1}\partial_t\mathbf{H}(\boldsymbol{\rho},t)\cdot\mathbf{H}(\boldsymbol{\rho},t)\Big\}ds \\ &+\int_{\Gamma_o}\Big\{\frac{1}{2c}\partial_t[\hat{\mathbf{n}}_o\times\mathbf{H}(\boldsymbol{\rho},t)]\cdot[\hat{\mathbf{n}}_o\times\mathbf{H}(\boldsymbol{\rho},t)] \\ &+\mathbf{H}(\boldsymbol{\rho},t)\cdot\mathbf{V}(\boldsymbol{\rho},t)\Big\}d\ell. \end{aligned} \tag{11}$$

To seek the solution of this variational problem using the FEM, Ω_o is first subdivided into small triangular elements. The field within each element is expanded as

$$\mathbf{H}(\boldsymbol{\rho},t)=\sum_{i=1}^{n}u_i(t)\mathbf{N}_i^e \tag{12}$$

where n denotes the number of basis functions per element and $\mathbf{N}_i^e$ and u_i denote the vector expansion functions and corresponding expansion coefficients, respectively. To obviate the need for a matrix solution in each time step, the $\mathbf{N}_i^e$ must be orthogonal

$$\langle\mathbf{N}_i^e,\mathbf{N}_j^e\rangle=\iint_{\Omega^e}\mathbf{N}_i^e\cdot\mathbf{N}_j^e d\Omega=\delta_{ij} \tag{13}$$

where Ω^e denotes the area of element e and δ_{ij} is the Kronecker delta function. Using numerical integration, (13) can be expressed as

$$\langle\mathbf{N}_i^e,\mathbf{N}_j^e\rangle=\sum_{\ell=1}^{3}\alpha_\ell\mathbf{N}_i^e(m_\ell)\cdot\mathbf{N}_j^e(m_\ell)=\delta_{ij} \tag{14}$$

where m_ℓ denotes the midpoint of edge ℓ of element e, and the coefficients α_ℓ are chosen such that the numerical integration is at least second-order accurate.

The most widely used vector basis functions for the finite element analysis of vector EM problems are the Whitney edge-based functions given by

$$\mathbf{W}_i^e=\lambda_j\nabla\lambda_k-\lambda_k\nabla\lambda_j \tag{15}$$

for edge i that connects nodes j and k, where λ_j and λ_k represent the standard linear nodal basis functions associated with nodes j and k, respectively. The $\mathbf{W}_i^e$ guarantee the tangential continuity of the fields across the element interfaces, while allowing for the normal discontinuity. Therefore, they can represent the fields correctly. However, these functions do not satisfy the orthogonality defined in (14). To make them orthogonal, as well as to preserve the property of tangential continuity, one first constructs vector basis functions $\mathbf{Z}_i^e$ that satisfy

$$\mathbf{Z}_i^e=\begin{cases}(\hat{\mathbf{t}}_i\cdot\mathbf{W}_i^e)\hat{\mathbf{t}}_i, & \text{at the midpoint of edge } i\\ \mathbf{0}, & \text{at the midpoints of other edges}\end{cases} \tag{16}$$

where $\hat{\mathbf{t}}_i$ represents the unit vector tangential to edge i. Clearly, $\mathbf{Z}_i^e$ so constructed satisfy (14). However, the $\mathbf{Z}_i^e$ cannot represent fields that have nonvanishing normal components at the midpoints of the element edges, hence, they form an incomplete set. To remedy this problem, another set of basis functions $\mathbf{B}_i^e$ is needed; these functions should satisfy

$$\mathbf{B}_i^e=\begin{cases}\hat{\mathbf{n}}_i, & \text{at the midpoint of edge } i\\ \mathbf{0}, & \text{at the midpoints of other edges}\end{cases} \tag{17}$$

where $\hat{\mathbf{n}}_i$ denotes the unit vector normal to edge i. Clearly, according to (14), the $\mathbf{B}_i^e$ so constructed are not only mutually orthogonal, but also orthogonal with respect to all $\mathbf{Z}_i^e$.

The requirements above do not uniquely determine the $\mathbf{Z}_i^e$ and $\mathbf{B}_i^e$. Here, White's [18] construction is adopted

$$\begin{aligned}\mathbf{B}_i^e=&\lambda_j\lambda_k\hat{\mathbf{n}}_i\\ \mathbf{Z}_i^e=&\mathbf{W}_i^e-\sum_{m=1}^{3}\frac{\langle\mathbf{W}_i^e,\mathbf{B}_m^e\rangle}{\langle\mathbf{B}_m^e,\mathbf{B}_m^e\rangle}\mathbf{B}_m^e.\end{aligned} \tag{18}$$

Using $\mathbf{Z}_i^e$ and $\mathbf{B}_i^e$ as the vector basis functions, (12) becomes

$$\mathbf{H}=\sum_{i=1}^{3}h_i(t)\mathbf{Z}_i^e+\sum_{i=1}^{3}b_i(t)\mathbf{B}_i^e. \tag{19}$$

By substituting (19) into (11), taking the partial derivatives of the functional with respect to the expansion coefficients and setting the resultant equations to zero, the following system of ordinary differential equations is obtained:

$$\mathbf{T}\frac{d^2u}{dt^2}+(\mathbf{R}+\mathbf{Q})\frac{du}{dt}+\mathbf{S}u+v=0. \tag{20}$$

Here u is a column vector consisting of unknown coefficients h_i and b_i, and $\mathbf{T}$, $\mathbf{R}$, and $\mathbf{S}$ are square matrices, assembled from their corresponding element matrices given by

$$\mathbf{T}^e = \begin{bmatrix} [\mu\langle \mathbf{Z}_i^e, \mathbf{Z}_j^e\rangle] & [0] \\ [0] & [\mu\langle \mathbf{B}_i^e, \mathbf{B}_j^e\rangle] \end{bmatrix} \tag{21}$$

$$\mathbf{R}^e = \begin{bmatrix} [\mu\sigma\epsilon^{-1}\langle \mathbf{Z}_i^e, \mathbf{Z}_j^e\rangle] & [0] \\ [0] & [\mu\sigma\epsilon^{-1}\langle \mathbf{B}_i^e, \mathbf{B}_j^e\rangle] \end{bmatrix} \tag{22}$$

$$\mathbf{S}^e = \begin{bmatrix} [\epsilon^{-1}\langle \nabla\times\mathbf{Z}_i^e, \nabla\times\mathbf{Z}_j^e\rangle] & [\epsilon^{-1}\langle \nabla\times\mathbf{Z}_i^e, \nabla\times\mathbf{B}_j^e\rangle] \\ [\epsilon^{-1}\langle \nabla\times\mathbf{B}_i^e, \nabla\times\mathbf{Z}_j^e\rangle] & [\epsilon^{-1}\langle \nabla\times\mathbf{B}_i^e, \nabla\times\mathbf{B}_j^e\rangle] \end{bmatrix}. \tag{23}$$

Matrix $\mathbf{Q}$ and vector v are contributed by the line integral along Γ_o. To be more specific, the element matrix $\mathbf{Q}^e$ is given by

$$\mathbf{Q}^e = \frac{1}{c}\begin{bmatrix} [\langle \hat{\mathbf{n}}_o\times\mathbf{Z}_i^e, \hat{\mathbf{n}}_o\times\mathbf{Z}_j^e\rangle] & 0 \\ 0 & 0 \end{bmatrix} \tag{24}$$

where the inner product involves the line integral along Γ_o. The vector v contains the discrete values of the tangential component of $\mathbf{V}$ on Γ_o.

Adopting a traditional central difference scheme to approximate the first- and second-order time derivatives in (20) yields

$$\mathbf{P}u^{n+1} = \left(\frac{2}{\Delta t^2}\mathbf{T} - \mathbf{S}\right)u^n + \left[\frac{1}{2\Delta t}(\mathbf{R}+\mathbf{Q}) - \frac{1}{\Delta t^2}\mathbf{T}\right]u^{n-1} - v^n \tag{25}$$

in which

$$\mathbf{P} = \frac{1}{\Delta t^2}\mathbf{T} + \frac{1}{2\Delta t}(\mathbf{R}+\mathbf{Q}) \tag{26}$$

and Δt represents the time step. Because of our usage of orthogonal vector basis functions, matrices $\mathbf{T}$, $\mathbf{R}$, and $\mathbf{Q}$, and hence $\mathbf{P}$, are diagonal. Consequently, the matrix solution at every time step is obviated. The time marching of (25) involves only a matrix-vector multiplication, which is efficient due to the sparseness of the matrix $\mathbf{S}$.

C. PWTD-Based Evaluation of Boundary Integrals

The above outlined FE–BI scheme requires the evaluation of $\mathbf{V}(\boldsymbol{\rho},t)$ (4) with $\mathbf{H}(\boldsymbol{\rho},t)$ replaced by $\tilde{\mathbf{H}}(\boldsymbol{\rho},t)$ (7) for observers $\boldsymbol{\rho}\in\Gamma_o$. The evaluation of $\tilde{\mathbf{H}}(\boldsymbol{\rho},t)$ in turn requires the computation of the magnetic and electric vector potentials $\mathbf{A}(\boldsymbol{\rho},t)$ and $\mathbf{F}(\boldsymbol{\rho},t)$ by spatial and temporal convolution of the electric and magnetic source densities $\mathbf{J}(\boldsymbol{\rho},t)$ and $\mathbf{K}(\boldsymbol{\rho},t)$ with the Green's function $g(\boldsymbol{\rho},t)$, respectively. To estimate the cost of these operations, let N_s and N_o denote the number of edges on Γ_s and Γ_o. In what follows, it is assumed that Γ_o closely adheres to Γ_s and therefore that $N_s \approx N_o$; that the source densities $\mathbf{J}(\boldsymbol{\rho},t)$ and $\mathbf{K}(\boldsymbol{\rho},t)$ can be discretized in terms of $O(N_s)$ samples; and that the FE–BI scheme is executed for a total of N_t time steps. Under these assumptions, the cost of the BI computation dominates that of the FE update. Indeed, the computational cost of evaluating $\mathbf{V}(\boldsymbol{\rho},t)$ at $O(N_o)$ points on Γ_o scales as $O(N_t^2N_s^2)$. This cost is entirely due to the spatial and temporal convolution requisite in the evaluation of $\mathbf{A}(\boldsymbol{\rho},t)$ and $\mathbf{F}(\boldsymbol{\rho},t)$; the computational costs of approximating $\mathbf{J}(\boldsymbol{\rho},t)$ and $\mathbf{K}(\boldsymbol{\rho},t)$ on Γ_s from the FE description of the magnetic field within Γ_o, evaluating $\tilde{\mathbf{H}}(\boldsymbol{\rho},t)$ from the potentials $\mathbf{A}(\boldsymbol{\rho},t)$ and $\mathbf{F}(\boldsymbol{\rho},t)$, and computing $\mathbf{V}(\boldsymbol{\rho},t)$ from $\tilde{\mathbf{H}}(\boldsymbol{\rho},t)$ all scale linearly in both N_t and N_s.

Here, the PWTD algorithm is used to accelerate the evaluation of $\mathbf{A}(\boldsymbol{\rho},t)$ and $\mathbf{F}(\boldsymbol{\rho},t)$. The PWTD algorithm is the extension of the frequency domain fast multipole method (Helmholtz equation) to the time domain (wave equation) and permits the evaluation of $\mathbf{A}(\boldsymbol{\rho},t)$ and $\mathbf{F}(\boldsymbol{\rho},t)$ for all observers and time steps in $O(N_t\log N_tN_s\log N_s)$ operations. The 2-D version of this algorithm is described in detail in [26]. Here, the algorithm's core ideas are summarized and its incorporation into the above-described FE–BI scheme outlined.

The 2-D PWTD scheme expresses fields due to line sources in terms of time-gated, Hilbert-transformed plane wave expansions. To rapidly evaluate the $\mathbf{A}(\boldsymbol{\rho},t)$ generated by $\mathbf{J}(\boldsymbol{\rho},t)$, the latter is broken up in space and time as

$$\mathbf{J}(\boldsymbol{\rho},t) = \sum_{n=1}^{N_s}\sum_{\nu=1}^{N_\nu}\mathbf{J}_n^\nu(\boldsymbol{\rho},t). \tag{27}$$

Source $\mathbf{J}_n^\nu(\boldsymbol{\rho},t)$ (i) resides on edge n on Γ_s, (ii) is bandlimited in time to $\omega_s = \chi_1\omega_{\max}$ where $\chi_1 > 1$ is a temporal oversampling factor and $\omega_{\max}$ is the highest frequency component (appreciably) present in the incident pulse, and (iii) is of essential duration T_s, that is, $\mathbf{J}_n^\nu(\boldsymbol{\rho},t)$ vanishes outside the temporal interval $[t_\nu^{\text{start}}, t_\nu^{\text{stop}}]$, where $t_\nu^{\text{stop}} - t_\nu^{\text{start}} = T_s\ \forall\nu$. It is assumed that the union of the temporal intervals $[t_\nu^{\text{start}}, t_\nu^{\text{stop}}]$ spans the duration of the analysis. A method for achieving this decomposition by interpolation using an approximate prolate series is described in [27]. Next, assume that source $\mathbf{J}_n^\nu(\boldsymbol{\rho},t)$ resides in a circle of radius R_s with center $\boldsymbol{\rho}_{c,n}$ and that the magnetic vector potential generated by this source is to be evaluated at observer $\boldsymbol{\rho}_m$ residing in a circle of like radius and center $\boldsymbol{\rho}_{c,m}$. It is assumed that $T_s < R_c - 2R_s$, where $R_c = |\mathbf{R}_c|$ and $\mathbf{R}_c = \boldsymbol{\rho}_{c,m} - \boldsymbol{\rho}_{c,n}$; in other words, no matter where $\mathbf{J}_n^\nu(\boldsymbol{\rho},t)$ is located within the source circle, its field cannot reach the observer circle before the source vanishes. Under these conditions, it can be shown that the vector potential generated by $\mathbf{J}_n^\nu(\boldsymbol{\rho},t)$ can be expressed as (28) shown at the bottom of the page, where

N_ϕ	$= \lceil 2\chi_2\chi_1\omega_{\max}R_s/c\rceil$;
$\chi_2 > 1$	angular oversampling ratio;
$\lceil\cdot\rceil$	denotes the nearest larger integer;
$\delta(\cdot)$	Dirac delta function;
$\hat{\mathbf{k}}(\phi)$	$= \hat{\mathbf{x}}\cos(\phi) + \hat{\mathbf{y}}\sin(\phi)$;

$$\mathbf{A}(\boldsymbol{\rho},t) \cong \begin{cases} \sum_{n=-N_\phi}^{+N_\phi}\delta\left[t - \frac{(\boldsymbol{\rho}_m - \boldsymbol{\rho}_{c,m})\cdot\hat{\mathbf{k}}(\phi_n)}{c}\right] * H\left\{\mathcal{T}_n[|\boldsymbol{\rho}_{c,m} - \boldsymbol{\rho}_{c,n}|, t] * \delta\left[t - \frac{(\boldsymbol{\rho}_{c,n} - \boldsymbol{\rho}_n)\cdot\hat{\mathbf{k}}(\phi_n)}{c}\right]\mathbf{J}_n^\nu(\boldsymbol{\rho},t)\right\} & t > t_\nu^{\text{stop}} \\ 0 & t \le t_\nu^{\text{stop}} \end{cases} \tag{28}$$

ϕ_n	$= 2\pi n/(2N_\phi + 1)$;
$*$	denotes temporal convolution;
H	Hilbert transform;
$\mathcal{T}_n(\boldsymbol{\rho}, t)$	translation function for direction n given by (29) at the bottom of the page.

Where $\epsilon_m = 2$ for $m = 0$ and $\epsilon_m = 1$ otherwise, ϕ_{cc} is the angle between the $\hat{\mathbf{x}}$ axis and the vector $\mathbf{R}_c$, and $T_m(\cdot)$ is the Chebyshev polynomial of degree m. Equation (29) implies that the magnetic vector potential generated by $\mathbf{J}_n^\nu(\boldsymbol{\rho}, t)$ can be constructed by 1) projecting the source density onto a discrete set of plane waves (outgoing rays) that radiate away from the source sphere, 2) Hilbert transforming the convolution of these outgoing rays with the translation functions $\mathcal{T}_n(\boldsymbol{\rho}, t)$ on a direction-by-direction basis, and 3) projecting the resulting incoming rays onto the observer. Fast methods for effecting step 2) are described in [26]. Strictly speaking, (29) only yields an approximation to the vector potential generated by $\mathbf{J}_n^\nu(\boldsymbol{\rho}, t)$; however, the error inherent in (29) decreases exponentially with increasing χ_1 and χ_2. The vector potential due to $\mathbf{J}(\boldsymbol{\rho}, t)$ can be obtained by summing up the contributions from all subsignals $\mathbf{J}_n^\nu(\boldsymbol{\rho}, t)$.

Equation (29) can be modified to directly yield the contribution of $\mathbf{J}_n^\nu(\boldsymbol{\rho}, t)$ to $\tilde{\mathbf{H}}(\boldsymbol{\rho}, t)$, or even $\mathbf{V}(\boldsymbol{\rho}, t)$. Indeed, the ∇ operators appearing in (4) and (5), when acting on ray n in expansion (29), can be replaced by $-\partial_t \hat{k}(\phi_n)/c$ and the action of all temporal derivatives can be incorporated into the translation functions $\mathcal{T}_n(\boldsymbol{\rho}, t)$. The resulting expressions are lengthy and, therefore, not reproduced here. Of course, the contribution to the electric vector potential $\mathbf{F}(\boldsymbol{\rho}, t)$ due to $\mathbf{K}_n^\nu(\boldsymbol{\rho}, t)$, the νth temporal subsignal describing the magnetic current on edge n, can be computed using the same techniques. It is important to note that while effecting the above PWTD translation processes, the contributions of $\mathbf{J}_n^\nu(\boldsymbol{\rho}, t)$ and $\mathbf{K}_n^\nu(\boldsymbol{\rho}, t)$ can be lumped into one scalar because a 2-D EM field is describable in terms of a single potential.

The PWTD scheme does not invoke the above described, three-stage sphere-to-sphere field translation algorithm separately for all source/observer pairs (m, n), but instead proceeds as follows. First, the domain bounded by Γ_o is encased in a square box. This box is recursively subdivided into four child boxes, a total of N_l times, until the area of the smallest boxes thus obtained is of $O(\lambda_{\min}^2)$, where $\lambda_{\min}$ is the free-space wavelength at $\omega_{\max}$. Parent boxes are said to exist at a higher level than their children. In addition, two nonempty boxes at any given level in the resulting tree are said to reside in each other's far-field provided that the distance between their centers equals at least twice their linear dimensions and their respective parents are not in each other's far field. Lowest level box pairs not accounted for by any far-field interaction are said to reside in each other's near field. Next, fields at all observers on Γ_o due to all far-field interactions are evaluated as follows:

1) *Construction of outgoing rays at all levels.* Outgoing rays for a given lowest-level box are computed by direct superposition of the contributions from all the electric and magnetic sources it contains. Outgoing rays for all higher-level boxes are computed by superposition of the interpolated and spliced ray spectra of their children. Interpolation ensures that rays at higher levels accurately describe the far-field spectra of higher-level boxes: the number of rays at any given level is proportional to the radius of the circle circumscribing a box at that level. Splicing ensures that the duration of subsignals translated between two boxes is always proportional to the distance between their centers divided by the speed of light.
2) *Construction of incoming rays at all levels.* Outgoing rays are translated between any pair of boxes that interact at a given level. This translation process requires the convolution of the outgoing rays with the translation function on a direction-by-direction basis and the evaluation of the Hilbert transform of the result. Again, both operations can be carried out fast (see [26]).
3) *Projection of the incoming rays associated with the fine grain boxes onto the observers.* Incoming rays at all levels are anterpolated (i.e., their density decreased) and resected (i.e., cut into shorter signals) before being propagated down the tree. Conceptually, these operations are the counterparts of the interpolation and splicing operators described above. Upon arrival at the lowest level in the tree, all rays are projected onto the observers.

All near-field interactions are accounted for using a special version of the algorithm that does not expand source fields in terms of plane waves but still relies on a Hilbert transform to efficiently represent the tail of the $g(\rho, t)$.

III. Numerical Examples

This section considers several examples that demonstrate the capabilities and accuracy of the proposed FE–BI algorithm. For all examples considered herein, the incident wave is a TMz Neumann pulse, viz., the time derivative of a Gaussian pulse

$$E_z^{\text{inc}}(\boldsymbol{\rho}, t) = 2\left[t - t_0 - c^{-1}\hat{\mathbf{k}} \cdot (\boldsymbol{\rho} - \boldsymbol{\rho}_0)\right] \times \exp\left\{-\frac{[t - t_0 - c^{-1}\hat{\mathbf{k}} \cdot (\boldsymbol{\rho} - \boldsymbol{\rho}_0)]^2}{\tau^2}\right\}. \quad (30)$$

Here $\hat{\mathbf{k}}$ is the direction of propagation of the incident pulse and t_0, $\boldsymbol{\rho}_0$, and τ are parameters that define the spectral and temporal reference points and shape.

The first example involves a perfect electrically conducting cylinder of radius 1.25 m (Fig. 2). The computational domain is discretized into 1284 triangular elements resulting in 5456

$$\mathcal{T}_n(\boldsymbol{\rho}, t) = \begin{cases} \frac{c}{2\pi(2N_\phi+1)R_c} \sum_{m=0}^{N_\phi} \epsilon_m \cos[m(\phi_{cc} - \phi_n)] \frac{T_m\left(\frac{ct}{R_c}\right)}{\sqrt{1-\left(\frac{ct}{R_c}\right)^2}} & -\frac{R_c}{c} < t < \frac{R_c}{c} \\ 0 & \text{elsewhere} \end{cases} \quad (29)$$

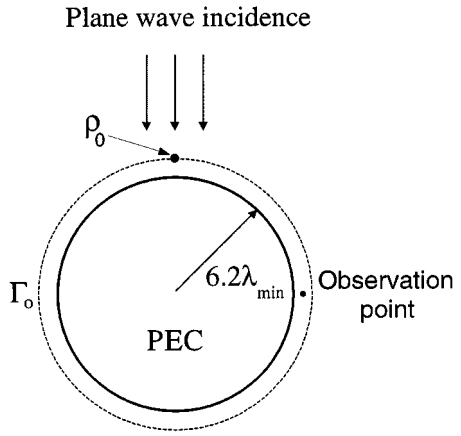

Fig. 2. A circular conducting cylinder under the plane wave incidence ($\lambda_{\min}$ denotes the minimum wavelength of the incident Neumann pulse).

unknowns and truncated by a circular boundary, which is placed two element layers away from the cylinder's surface. The pulse parameters are $\hat{\mathbf{k}} = -\hat{\mathbf{y}}$, $t_0 = 9.755$ ns, $\boldsymbol{\rho}_0 = 1.3\hat{\mathbf{y}}$ m, and $\tau = 1.971$ ns. The source boundary is placed between the conducting surface and the truncation boundary. Fig. 3 shows the temporal signature of the total magnetic field at $\boldsymbol{\rho} = 1.275\hat{\mathbf{x}} - 0.01\hat{\mathbf{y}}$ m. Comparison of the computed and the theoretical results reveals excellent agreement.

To demonstrate the present algorithm's ability to analyze complex geometries, a deep conducting cavity with width 1.25 m, length 2.5 m, and conductor thickness 0.25 m is considered next (Fig. 4.) The parameters defining the incident pulse are $\hat{\mathbf{k}} = \cos(135°)\hat{\mathbf{x}} + \sin(135°)\hat{\mathbf{y}}$, $t_0 = 8.31$ ns, $\boldsymbol{\rho}_0 = 2.6\hat{\mathbf{x}}$ m, and $\tau = 1.679$ ns. The mesh truncation boundary follows the cavity outline and is positioned two elements away from its surface. The simulation domain is subdivided into 2440 patches, yielding 10 371 unknowns. The same scattering problem is also analyzed using a FDTD solver that truncates the computational domain with a perfectly matched layer (PML). This solver requires that the computational domain include the cavity's interior as the PML cannot be attached to concave outer boundaries. This, of course, artificially inflates the number of unknowns in the FDTD solver. The temporal signatures of the magnetic field sampled at $\boldsymbol{\rho} = 0.035\hat{\mathbf{x}} + 0.025\hat{\mathbf{y}}$ m and $\boldsymbol{\rho} = 0.616\hat{\mathbf{x}} + 1.025\hat{\mathbf{y}}$ m are shown in Fig. 5. The results obtained with the FE–BI scheme agree very well with those obtained from the FDTD solver. A slight discrepency in Fig. 5(a) is due to the error in the FDTD solution caused by PML.

Next, to illustrate the capability of the present algorithm to handle materials as well as complex geometries, a dielectric cavity is considered. This cavity has the same cross section as the one considered in the previous example and its material has a relative dielectric permittivity of 4.0. The outer boundary is constructed as in the example above. The computational region is discretized into 7412 patches, generating 33 106 unknowns. The incidence direction is the same as the previous example and the pulse parameters are $t_0 = 10.1$ ns, $\boldsymbol{\rho}_0 = 2.6\hat{\mathbf{x}}$ m, and $\tau = 2.042$ ns. Fig. 6 shows the calculated total magnetic field at $\boldsymbol{\rho} = 0.0375\hat{\mathbf{x}} + 0.025\hat{\mathbf{y}}$ m and $\boldsymbol{\rho} = 0.6125\hat{\mathbf{x}} + 1.025\hat{\mathbf{y}}$ m; again, the results obtained using the FE–BI method agree very well with those obtained using the FDTD solver.

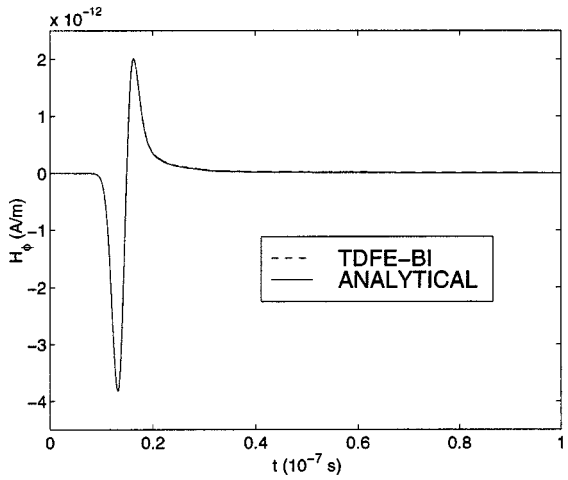

(a)

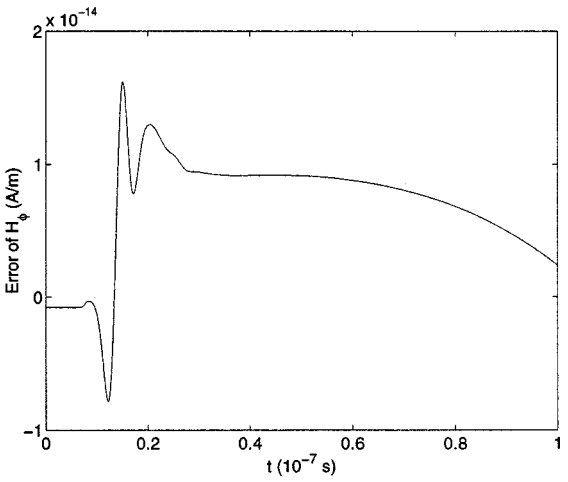

(b)

Fig. 3. Scattering by a circular conducting cylinder. (a) H_ϕ. (b) Absolute error in H_ϕ.

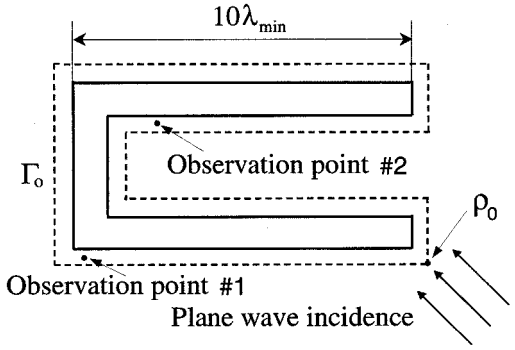

Fig. 4. A perfect conducting cavity under the plane wave incidence ($\lambda_{\min}$ denotes the minimum wavelength of the incident Neumann pulse).

Finally, to compare the efficiency and accuracy of the present method with the FDTD solver, we considered the problem of wave scattering by a coated cylinder having a radius of 0.2 m. The coating has a thickness of 0.008 m and a relative permittivity of $\epsilon_r = 16$. For the TDFEM computation, the comput-

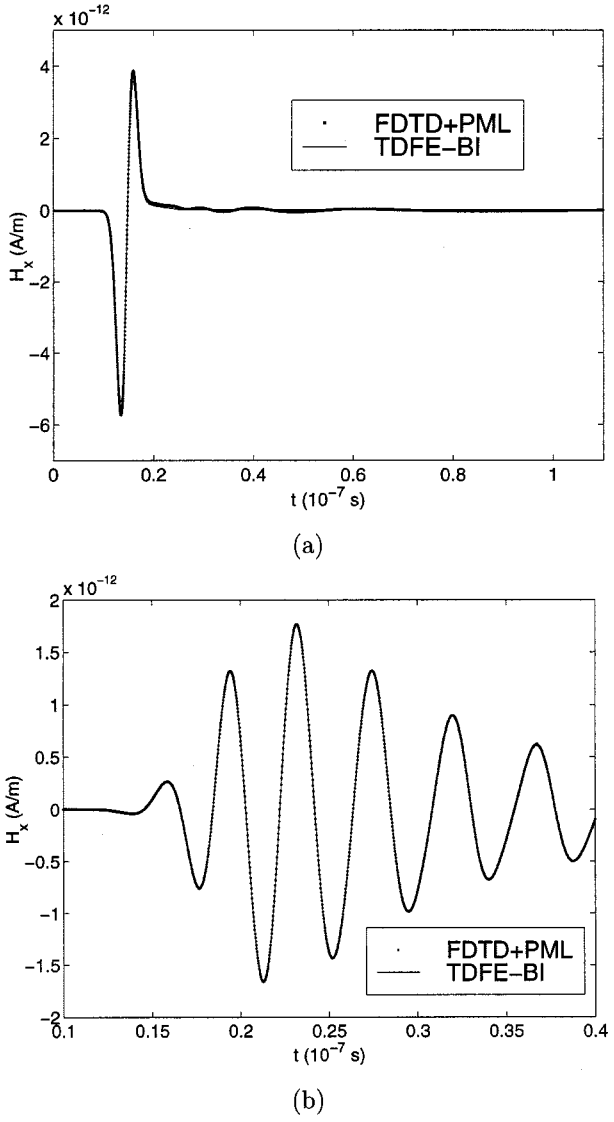

Fig. 5. Scattering by a conducting cavity with width $5\ \lambda_{\min}$, length $10\ \lambda_{\min}$, and conductor thickness $1\ \lambda_{\min}$. (a) H_x at observation point $\#1$. (b) H_x at observation point $\#2$.

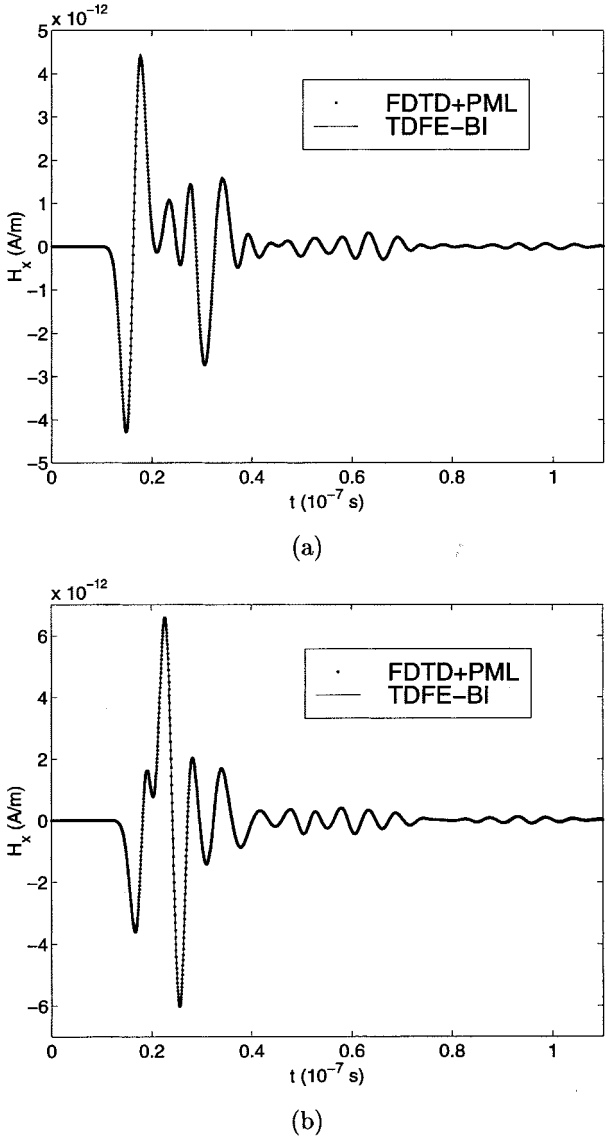

Fig. 6. Scattering by a dielectric cavity with width $5\ \lambda_{\min}$, length $10\ \lambda_{\min}$, and dielectric thickness $1\ \lambda_{\min}$. (a) H_x at observation point $\#1$. (b) H_x at observation point $\#2$.

ational domain is truncated at two elements away from the dielectric surface and is discretized into 2298 triangular elements, yielding 10 051 unknowns. For the FDTD simulation, the cylinder is enclosed in a square region, which is then discretized into square grids of size 0.004 m. The pulse parameters for the excitation are $\hat{\mathbf{k}} = -\hat{\mathbf{y}}$, $t_0 = 1.57$ ns, $\boldsymbol{\rho}_0 = 0.216\hat{\mathbf{y}}$ m, and $\tau = 0.32$ ns. To make the comparison meaningful, both the TDFEM and FDTD use the exact BI, evaluated by the PWTD algorithm, at the truncation boundary. (The use of PWTD in the FDTD is described in detail by Lu *et al.* [28].) The average and maximum errors in the FDTD calculation of the E_z at a fixed point ($\boldsymbol{\rho} = -0.208\hat{\mathbf{x}} - 0.0025\hat{\mathbf{y}}$ m) are 5.61% and 56.34%, respectively, relative to the peak value of E_z, whereas those in the TDFE calculation are only 0.28% and 2.72%, respectively. The larger error in the FDTD calculation is caused by the staircase approximation of the scatterer's geometry, which is absent in the TDFE simulation. Of course, such a staircase approximation can be removed using more complicated FDTD algorithms that are based on irregular grids. The computing time and memory usage are approximately the same for the TDFE and FDTD calculations because they are dominated by the PWTD algorithm.

IV. Conclusion

A novel hybrid FE–BI method for analyzing transient scattering from freestanding 2-D inhomogeneous objects was presented. The FE component of the solver utilized a pair of orthogonal vector basis functions to model the fields in the interior of the computational domain. The interior FE and exterior BI field models were coupled to each other using a novel scheme that yields solutions free of spurious modes. The orthogonality of the FE basis functions and the nature of the FE–BI coupling

scheme obviated the need for any matrix inversion during the time stepping process. Finally, all BIs are evaluated using the PWTD algorithm, which reduces the computational complexity of the algorithm. The method's capabilities and accuracy were demonstrated by several numerical examples. The formulation was based on vector finite elements and, therefore, can be extended readily to three dimensions.

REFERENCES

[1] P. P. Silvester and G. Pelosi, Eds., *Finite Elements for Wave Electromagnetics*. New York: IEEE Press, 1994.

[2] K. S. Yee, "Numerical solution of initial boundary value problems involving Maxwell's equations in isotropic media," *IEEE Trans. Antennas Propagat.*, vol. AP-14, pp. 302–307, May 1966.

[3] R. Mittra, "Integral equation methods for transient scattering," in *Transient Electromagnetic Fields*, L. B. Felsen, Ed. New York; Berlin, Germany; Vienna, Austria: Springer-Verlag, 1976, ch. 2.

[4] A. C. Cangellaris, C. C. Lin, and K. K. Mei, "Point-matched time-domain finite element methods for electromagnetic radiation and scattering," *IEEE Trans. Antennas Propagat.*, vol. AP-35, pp. 1160–1173, Oct. 1987.

[5] J. T. Elson, H. Sangani, and C. H. Chan, "An explicit time-domain method using three-dimensional Whitney elements," *Microwave Opt. Tech. Lett.*, vol. 7, no. 13, pp. 607–610, Sept. 1994.

[6] T. V. Yioultsis, N. V. Kantartzis, C. S. Antonopoulos, and T. D. Tsiboukis, "A fully explicit Whitney element-time domain scheme with higher order vector finite elements for three-dimensional high frequency problems," *IEEE Trans Magn.*, vol. 34, pp. 3288–3291, Sept. 1998.

[7] M. Feliani and F. Maradei, "Hybrid finite element solution of time dependent Maxwell's curl equations," *IEEE Trans. Magn.*, vol. 31, pp. 1330–1335, May 1995.

[8] K. Choi, S. J. Salon, K. A. Connor, L. F. Libelo, and S. Y. Hahn, "Time domain finite element analysis of high power microwave aperture antennas," *IEEE Trans. Magn.*, vol. 31, pp. 1622–1625, May 1995.

[9] M. Hano and T. Itoh, "Three-dimensional time-domain method for solving Maxwell's equations based on circumference of elements," *IEEE Trans. Magn.*, vol. 32, pp. 946–949, May 1996.

[10] A. Bossavit and I. Mayergoyz, "Edge elements for scattering problems," *IEEE Trans. Magn.*, vol. 25, pp. 2816–2821, July 1989.

[11] M. F. Wong, O. Picon, and V. F. Hanna, "A finite-element method based on Whitney forms to solve Maxwell's equations in the time domain," *IEEE Trans. Magn.*, vol. 31, pp. 1618–1621, May 1995.

[12] K. Mahadevan and R. Mittra, "Radar cross section computation of inhomogeneous scatterers using edge-based finite element methods in frequency and time domains," *Radio Sci.*, vol. 28, no. 6, pp. 1181–1193, Nov.–Dec. 1993.

[13] D. R. Lynch and K. D. Paulsen, "Time-domain integration of the Maxwell equations on finite elements," *IEEE Trans. Antennas Propagat.*, vol. 38, pp. 1933–1942, Dec. 1990.

[14] G. Mur, "The finite-element modeling of three-dimensional time-domain electromagnetic fields in strongly inhomogeneous media," *IEEE Trans. Magn.*, vol. 28, pp. 1130–1133, Mar. 1992.

[15] J. F. Lee and Z. Sacks, "Whitney elements time domain (WETD) methods," *IEEE Trans. Magn.*, vol. 31, pp. 1325–1329, May 1995.

[16] J. F. Lee, "WETD-A finite-element time-domain approach for solving Maxwell's equations," *IEEE Microwave Guided Wave Lett.*, vol. 4, pp. 11–13, Jan. 1994.

[17] S. D. Gedney and U. Navsariwala, "An unconditionally stable finite-element time-domain solution of the vector wave equation," *IEEE Microwave Guided Wave Lett.*, vol. 5, pp. 332–334, Oct. 1995.

[18] D. A. White, "Orthogonal vector basis functions for time domain finite element solution of the vector wave equation," *IEEE Trans. Magn.*, vol. 35, pp. 1458–1461, May 1999.

[19] J. M. Jin, M. Zunoubi, K. C. Donepudi, and W. C. Chew, "Frequency-domain and time-domain finite-element solution of Maxwell's equations using spectral Lanczos decomposition method," *Comput. Methods Appl. Mech. Eng.*, vol. 169, pp. 279–296, 1999.

[20] J. F. Lee, R. Lee, and A. Cangellaris, "Time-domain finite-element methods," *IEEE Trans. Antennas Propagat.*, vol. 45, pp. 430–442, Mar. 1997.

[21] J. R. Brauer, R. Mittra, and J. F. Lee, "Absorbing boundary condition for vector and scalar potentials arising in electromagnetic finite element analysis in frequency and time domains," in *IEEE APS Int. Symp. Dig.*, 1991, pp. 1224–1227.

[22] K. Mahadevan, R. Mittra, D. Rowse, and J. Murphy, "Edge-based finite element frequency and time domain algorithms for RCS computation," in *IEEE APS Int. Symp. Dig.*, vol. 3, 1993, pp. 1680–1683.

[23] T. V. Yioultsis, T. D. Tsiboukis, and E. E. Kriezis, "A generalized non-diagonally anisotropic perfectly matched layer for wide-angle absorption in finite element electromagnetic scattering analysis," *IEEE Trans. Magn.*, vol. 34, pp. 2732–2735, Sept. 1998.

[24] A. F. Peterson, "The interior resonance problem associated with surface integral equations of electromagnetics: Numerical consequences and a survey of remedies," *Electromagn.*, vol. 10, no. 3, pp. 293–312, July–Sept. 1990.

[25] J. M. Jin, *The Finite Element Method in Electromagnetics*. New York: Wiley, 1993.

[26] M. Lu, J. Wang, A. A. Ergin, and E. Michielssen, "Fast evaluation of two-dimensional transient wave fields," *J. Comput. Phys.*, vol. 158, pp. 161–185, 2000.

[27] J. J. Knab, "Interpolation of bandlimited functions using the approximate prolate series," *IEEE Trans. Inform. Theory*, vol. 25, pp. 717–718, 1979.

[28] M. Lu, A. A. Ergin, B. Shankar, and E. Michielssen, "Global absorbing boundary condition for 2D FDTD simulations based on the multi-level plane wave time domain algorithm," Dept. Elect. Comp. Eng., Univ. of Illinois, Internal Tech. Rep., 1999.

Dan Jiao was born in Anhui Province, China, in 1972. She received the B.S. and M.S. degrees in electrical engineering from Anhui University, China, in 1993 and 1996, respectively. From 1996 to 1998, she performed graduate studies at the University of Science and Technology of China, Hefei, China. She is currently working toward the Ph.D. degree in electrical engineering at the University of Illinois at Urbana-Champaign.

Since 1998, she has been a Research Assistant at the Center for Computational Electromagnetics, University of Illinois at Urbana-Champaign.

Ms. Jiao was the recipient of the 2000 Raj Mittra Outstanding Research Award presented by the Department of Electrical and Computer Engineering, University of Illinois at Urbana-Champaign. Her current research interests include fast computational methods in electromagnetics and time-domain numerical techniques.

Mingyu Lu was born in Beijing, China, in 1972. He received the B.S. and M.S. degrees in electrical engineering from Tsinghua University, Beijing, China, in 1995 and 1997, respectively. He is currently working toward the Ph.D. degree in electrical engineering at the University of Illinois at Urbana-Champaign.

Since 1997, he has been a research assistant at the Center for Computational Electromagnetics, University of Illinois at Urbana-Champaign. His current research interests include fast transient integral equation solver for electromagnetic analysis.

Eric Michielssen (M'95–SM'99) received the M.S. degree in electrical engineering (*summa cum laude*) from the Katholieke Universiteit Leuven (KUL), Belgium, and the Ph.D. degree in electrical engineering from the University of Illinois at Urbana-Champaign (UIUC) in 1987 and1992, respectively.

From 1987 to 1988, he was a Research and Teaching Assistant in the Microwaves and Lasers Laboratory with KUL. From 1988 to 1992, he was with the Electromagnetic Communication Laboratory at UIUC, also as a Research and Teaching Assistant. In 1992, he joined the Faculty of the Department of Electrical and Computer Engineering at the University of Illinois as a Visiting Assistant Professor. In 1993, he was appointed Assistant Professor of Electrical and Computer Engineering and in 1998 he was promoted to Associate Professor. Since 1995, he has served as Associate Director of the Center for Computational Electromagnetics at UIUC. He is author or coauthor of over 70 journal papers and book chapters and over 100 papers in conference proceedings. His research interests include all aspects of theoretical and applied computational electromagnetics. His principal research focus has been the development of fast frequency and time domain integral-equation-based techniques for analyzing electromagnetic phenomena, and the development of robust, genetic algorithm driven optimizers for the synthesis of electromagnetic devices.

Dr. Michielssen received a Belgian American Educational Foundation Fellowship in 1988 and a Schlumberger Fellowship in 1990. He was the recipient of a 1994 International Union of Radio Scientists (URSI) Young Scientist Fellowship, a 1995 National Science Foundation CAREER Award, and the 1998 Applied Computational Electromagnetics Society (ACES) Valued Service Award. He was named 1999 URSI United States National Committee Henry G. Booker Fellow and selected as the recipient of the 1999 URSI Koga Gold Medal. In 1997, he served as the Technical Chairman of the Applied Computational Electromagnetics Society (ACES) Symposium (REVIEW OF PROGRESS IN APPLIED COMPUTATIONAL ELECTROMAGNETICS, Monterey, CA, March 1997), and currently serves on the ACES Board of Directors and as ACES Vice-President. From 1997 to 1999, he was as an Associate Editor for Radio Science and is currently an Associate Editor for the IEEE TRANSACTIONS ON ANTENNAS AND PROPAGATION. He is a member of URSI Commission B.

Jian-Ming Jin (S'87–M'89–SM'94–F'01) received the B.S. and M.S. degrees in applied physics from Nanjing University, Nanjing, China, and the Ph.D. degree in electrical engineering from the University of Michigan, Ann Arbor, in 1982, 1984, and 1989, respectively.

Currently, he is a Professor of Electrical and Computer Engineering and Associate Director of the Center for Computational Electromagnetics at the University of Illinois at Urbana-Champaign. He is author or coauthor of over 110 papers in refereed journals and 15 book chapters. He is author of *The Finite Element Method in Electromagnetics* (New York: Wiley, 1993) and *Electromagnetic Analysis and Design in Magnetic Resonance Imaging* (Boca Raton, FL: CRC, 1998). He is coauthor of *Computation of Special Functions* (New York: Wiley, 1996), and coedited *Fast and Efficient Algorithms in Computational Electromagnetics* (Norwood, MA: Artech, 2001). His current research interests include computational electromagnetics, scattering and antenna analysis, electromagnetic compatibility, and magnetic resonance imaging. His name is often listed in the University of Illinois at Urbana-Champaign's *List of Excellent Instructors.* He currently serves as an Associate Editor of *Radio Science* and is also on the Editorial Board for *Electromagnetics Journal* and *Microwave and Optical Technology Letters*.

Dr. Jin is a member of Commision B of USNC/URSI, Tau Beta Pi, and International Society for Magnetic Resonance in Medicine. He was a recipient of the 1994 National Science Foundation Young Investigator Award and the 1995 Office of Naval Research Young Investigator Award. He also received the 1997 Xerox Junior Research Award and the 2000 Xerox Senior Research Award presented by the College of Engineering, University of Illinois at Urbana-Champaign. In 1998 he was appointed the first Henry Magnuski Outstanding Young Scholar in the Department of Electrical and Computer Engineering. He was a Distinguished Visiting Professor in the Air Force Research Laboratory in 1999. From 1996 to 1998 he served as an Associate Editor of the IEEE TRANSACTIONS ON ANTENNAS AND PROPAGATION. He was the Co-Chairman and Technical Program Chairman of the Annual Review of Progress in Applied Computational Electromagnetics in both 1997 and 1998.